ACS MATERIALS LETTERS

www.acsmaterialsletters.org

3D-Printable Elastomers for Real-Time Autonomous Self-Healing in Soft Devices

Joseph G. Beckett, Carl J. Thrasher,* Joshua Michonski, Robert M. Drexler, Sachin Babu, Allyson M. Cox, Braeden J. Windham, Zhenning Yu, Anesia D. Auguste, Abhishek Shetty, Timothy H. Osborn, Robert L. Lowe,* Laura A. Sowards, and Christopher A. Crouse*

Cite This: ACS Materials Lett. 2025, 7, 123−132

Read Online

ACCESS | Metrics & More | Article Recommendations | Supporting Information

ABSTRACT: **Photocurable self-healing elastomers are promising candidates for producing complex soft devices that can mend damage. However, the practicality of these materials is limited by reliance on external stimuli, custom synthesis, manual realignment, and multihour healing cycles. This paper introduces a tough 3D-printable hybrid acrylate/thiol-ene elastomer (prepared with commercially available precursors) that exhibits nearly instantaneous damage repair in the absence of external stimuli. This rapid, hydrogen bond-driven self-healing enables meaningful restoration of mechanical properties, including tensile strains up to 344% post-damage. Furthermore, structured herringbone grafts are showcased as a compelling strategy to enable cohesive failure away from healed interfaces, realizing up to 18× increases in toughness from only modest increases in interfacial surface area. Prototype soft robotic devices fabricated using vat photopolymerization demonstrate self-healing within seconds under ambient conditions and without external intervention. These results demonstrate a scalable strategy to provide real-time, autonomous functionality restoration in damaged soft devices.**

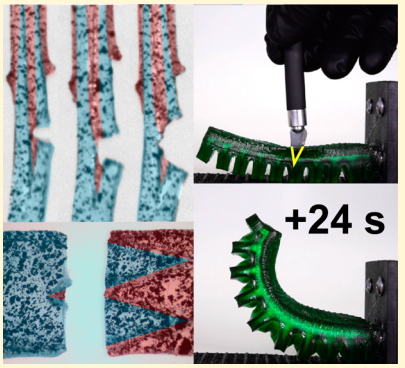

Emerging human-interfacing technologies such as soft actuators,[1,2] stretchable sensors,[3,4] tissue grafts,[5] and compliant energy harvesting devices[6,7] are distinguished by their reliance on soft elastomeric materials. Complex multimaterial interfaces and intricate structuring are often used to enhance the capabilities of these devices, but simultaneously pose fabrication and resiliency challenges. These tradeoffs are balanced by soft biological structures, which use self-healing to mitigate vulnerability to externally induced damage. While synthetic soft materials with impressive mechanical properties and self-healing capabilities have been demonstrated,[8−14] it remains difficult to fabricate intricate devices with these typically molded materials. Although recent advances such as joining preformed components and direct-write printing of self-healing materials have enabled some progress,[15−18] geometric complexity (e.g., overhangs, internal cavities) and resolution remain limiting factors for the production of practical self-healing devices.

A promising route to fabricate complex soft devices is vat photopolymerization (VP) additive manufacturing, where photocurable resins are iteratively irradiated with patterned light to form a three-dimensional (3D) part layer-by-layer.[19−21] This method can create intricate geometries with both high resolution and throughput, but synthesizing 3D-printable elastomeric resins with suitable mechanical properties and self-healing capacity has proven difficult.[22] While photocurable elastomers with self-healing efficiencies greater than 80% may be found, only a few exceed an ultimate tensile strength of 1 MPa.[23−25] Further, the best-performing materials utilize custom precursors to enable their self-healing, a factor that limits their scalability and utility outside of specialized laboratory environments. Beyond this, most 3D-printed self-healing materials suffer from long healing times and require external intervention to initiate the self-healing process. These interventions typically involve continuous exposure to an external stimulus (e.g., heat, light) and manual application of directional pressure.[26−28] Taken together, these factors greatly limit the practical utility of currently available 3D-printed self-healing materials.

To bridge the gap between manufacturing, performance, and utility in self-healing materials, we introduce a rapidly self-healing photocurable elastomeric hydrogel—comprised of commercial off-the-shelf (COTS) precursors—with robust mechanical properties. These materials exploit hybrid acrylate/thiol-ene chemistry to print tough materials with

Received: July 3, 2024
Revised: October 17, 2024
Accepted: October 29, 2024
Published: December 3, 2024

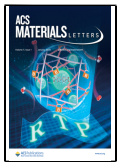

https://doi.org/10.1021/acsmaterialslett.4c01358
ACS Materials Lett. 2025, 7, 123−132

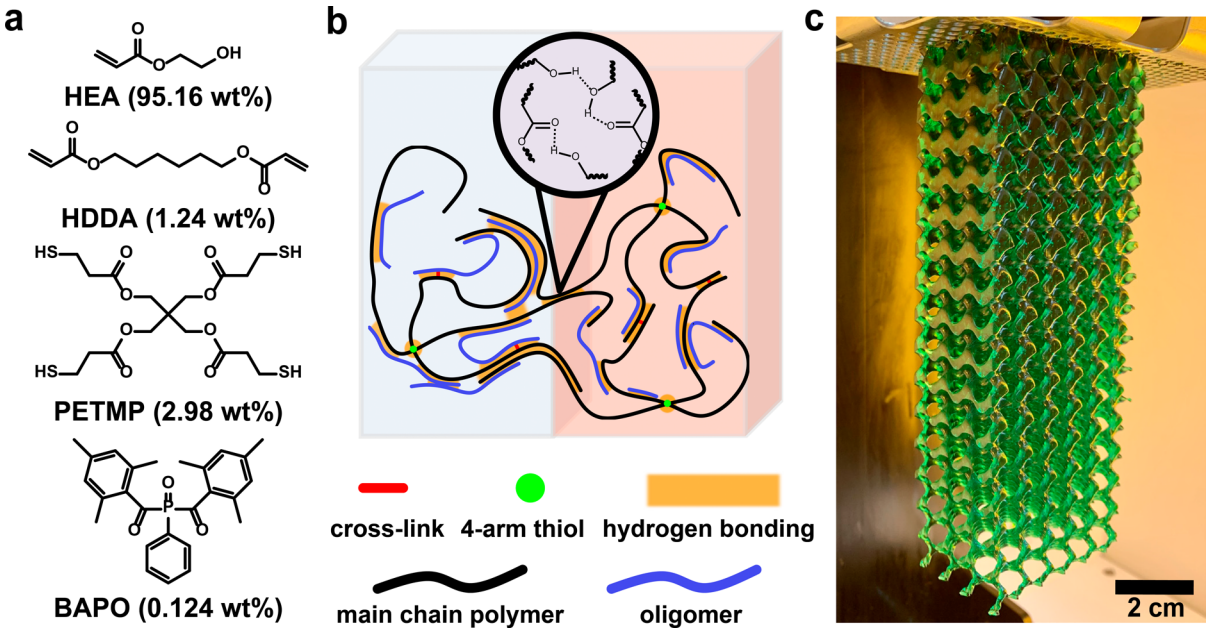

Figure 1. Resin composition and 3D printing. (a) Molecular structure of monomer (HEA), cross-linker (HDDA), 4-arm thiol (PETMP), and photoinitiator (BAPO). Compositions shown are for the DLP-printed resin, which also includes 0.497 wt % water-based green food dye. (b) Chain-network graphic illustrating pristine and self-healed bonding states. All damage repair is enabled using rapid hydrogen bonding. (c) 14.7-cm-tall gyroid lattice with continuously varying infill density (60% to 5% from top to bottom) printed on a commercial 3D Systems Figure 4 DLP 3D printer. The 130-g print was completed in 6 h and 21 min, with no visible defects.

elongations of 355% ± 33%, ultimate tensile stresses of 1.30 ± 0.27 MPa, and rapid hydrogen bond-mediated self-adhesion. To enable modular and reconfigurable devices, grafted interfaces were structured to ensure cohesive fracture away from self-healed interfaces, yielding up to a factor of 18 improvement in toughness over flat interfaces. The fracture mechanics of grafted specimens were investigated using full-field optical measurements via digital image correlation (DIC), which revealed self-amplifying interfacial strengthening with strain. These materials are robustly printable, as demonstrated by high-resolution prints as large as 6 cm × 3.9 cm × 14.7 cm (130 g) produced on commercial digital light processing (DLP) 3D-printing equipment. Pneumatic actuators printed from the resin exhibited nearly instantaneous, autonomous functionality restoration after being subjected to a razor puncture. The combined advances in 3D-printable self-healing materials and interfacial design of elastomeric grafts described herein showcase a scalable method to provide real-time healing capabilities in complex form factor soft devices.

■ POLYMER SYNTHESIS AND FABRICATION

The resin system was designed to be easily produced at scale, using only COTS chemicals. The composition of the resin includes a hydrogen-bonding monomer 2-hydroxyethyl acrylate (HEA) (95.16 wt %), dual chain-transfer agent and cross-linker pentaerythritol tetrakis(3-mercaptopropionate) (PETMP) (2.98 wt %), hexanediol diacrylate (HDDA) (1.24 wt %) cross-linker, and phenylbis(2,4,6-trimethylbenzoyl)phosphine oxide (BAPO) (0.124 wt %) as the photoinitiator (see Figure 1a, as well as Table S1 and Scheme S1 in the Supporting Information). Water-based green food dye (0.497 wt %) was used to prevent overpenetration of light during printing, thereby improving the quality and resolution of printed surfaces, sharp corners, and other fine features (see Figure S1 and Scheme S2 in the Supporting Information). All components were combined and subsequently mixed under ambient conditions. All curing was done in the presence of oxygen.

The enhanced self-healing performance of this material compared to similar material systems is primarily due to the thiol additive (see Scheme S3 in the Supporting Information). During free-radical polymerization, 4-arm thiols serve as chain-transfer agents that terminate propagating chains and reinitiate from a thiol-centered radical. This results in the creation of shorter oligomeric species in addition to larger 4-arm polymers, thereby broadening the molecular weight distribution.[29,30] The low-molecular-weight oligomers which account for roughly a third of the hydrogel mass (see Note S1 in the Supporting Information) act as plasticizers, yielding a lower Young's modulus and greater energy dissipation capacity (see Figure 1b and Figure S2 in the Supporting Information). These changes provide a tackiness in addition to the hydrogen bonding interactions of poly(2-hydroxyethyl acrylate) that, in imitating strategies used for adhesives, can increase interfacial bonding strength and provide fast self-healing rates.[31−34] While dynamic thioether exchange at elevated temperatures can also be used to support healing,[35] experiments suggest that the self-healing of the material reported herein is solely due to rapid adhesion-based hydrogen bonding (see Figure S3 in the Supporting Information). Although the addition of chain-transfer agents during polymerization typically results in reduced mechanical properties, the system described herein uses tetra-functional thiol moieties to produce additional crosslinks that mitigate the deleterious effects on mechanical properties while simultaneously enhancing adhesion. The end result is a self-healing hydrogel elastomer suitable for rapid photopolymerization-based 3D-printing processes with attractive mechanical properties well-suited for soft robotic applications and adhesion-based instantaneous self-healing.

As thiol and acrylate components are known to react spontaneously at ambient temperatures,[36] resin aging studies

https://doi.org/10.1021/acsmaterialslett.4c01358
ACS Materials Lett. 2025, 7, 123−132

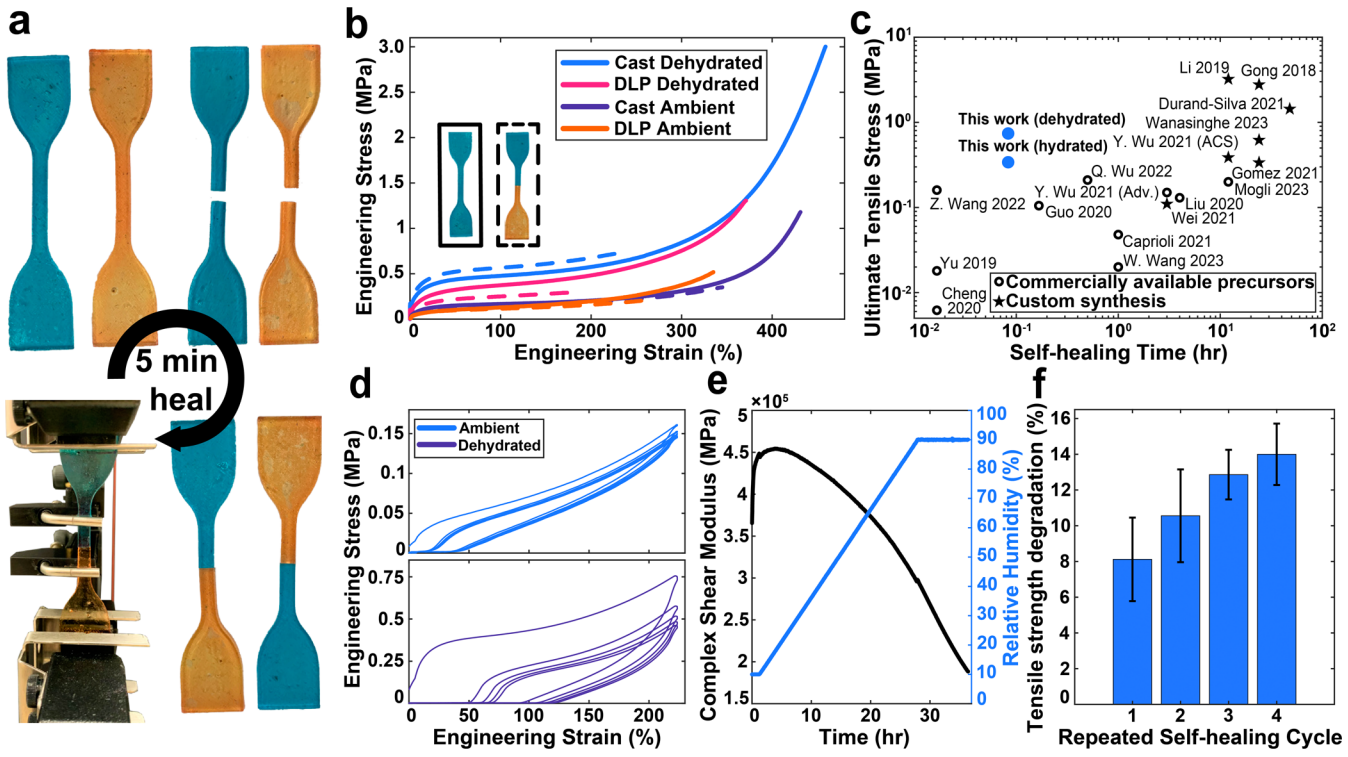

Figure 2. Pristine and self-healed material testing. (a) Self-healing procedure for damaged samples. Note that pieces are swapped between specimens to facilitate visualization of the healed interface. (b) Stress−strain curves (from uniaxial tension testing at a loading rate of 500 mm/min ≈ 0.1/s) for pristine (solid lines) and self-healed (dashed lines) materials with varying hydrogel water content and fabrication techniques. (c) Rapid hydrogen-bonding self-healing in the absence of external stimuli provided extremely competitive healing rate and ultimate tensile stress (UTS). Plot includes UTS values at shortest-reported self-healing time in each paper for photocured intrinsically self-healing elastomers. Materials with pristine strains less than 50% were excluded. (d) Cyclic tension testing illustrates minimal viscoelasticity in the ambiently stored (45% ± 20% RH) cast material. Reduced water content in the dehydrated samples (15% RH) leads to more prominent hysteresis. Each test consisting of five displacement-controlled cycles was conducted from 0 to ∼225% strain. (e) Long-duration continuous humidity sweep from 10 to 90% RH demonstrated a highly tunable modulus. (f) Repeated self-healing tests reveal only a 14% reduction in adhesive force over a series of four healing cycles, suggesting suitability of the material for use in reconfigurable devices.

were conducted via uniaxial tension tests on samples cured from resin stored under cold and room-temperature conditions. Results of these experiments (see Figure S4 in the Supporting Information) illustrate that storing the uncured resin at −20 °C prevents meaningful changes to the mechanical properties of the cured material. This suggests that sufficiently low storage temperatures minimize prereactions between the acrylate and thiol components. If, instead, the resin is stored at room temperature, we found that the resin should be cured within 2 days of mixing for optimal as-cured mechanical properties. Thus, the results reported herein were all obtained using resin cured within 24 h of mixing for cast samples and less than 48 h for printed samples.

The material was 3D printed under ambient conditions on a stock 3D Systems Figure 4 Modular DLP printer. DLP is a type of vat photopolymerization that uses projected light to cure full layers of resin simultaneously, which enables rapid print speeds. A 6.0 cm × 3.9 cm × 14.7 cm gyroid lattice was fabricated in just 6 h and 21 min, using a fine layer height of 50 μm (Figure 1c). The lattice was designed with an infill pattern that continuously varied in density from 60% at the top to 5% at the bottom, yielding a large 130g print.[37] This large-scale print produced a consistent surface finish with no visible signs of defects, even in regions with overhangs and fine features. A time lapse of the print was recorded and shown at 1600× speed (Video S1 in the Supporting Information). The material's print quality was very repeatable, even on complex objects with overhangs like the standard 3D "Benchy" test print (Figure S5 in the Supporting Information).

MECHANICAL CHARACTERIZATION

For mechanical characterization efforts, tensile specimens were produced using both casting and DLP 3D printing. After curing, all samples were stored for 7 days in a UV-protected environment at room temperature to achieve steady-state water content (Figure S6 in the Supporting Information), resulting in repeatable stress−strain curves across many samples (Figures S7 and S8 and Table S2 in the Supporting Information). As the material explored herein is a hydrophilic elastomer, mechanical properties were investigated as a function of humidity. Hydrated samples were stored at 45% ± 20% relative humidity (RH) in ambient air where they equilibrated to ∼2.7% water by mass, while dehydrated samples were stored in a nitrogen-purged desiccator at 15% RH where they equilibrated to ∼1.1% water by mass (Note S2 in the Supporting Information). To evaluate self-healing capacity, pristine and self-healed tensile specimens were characterized using uniaxial tension testing. All self-healed samples were fractured perpendicularly across the center of the specimen (Figure 2a) using a clean razor blade. Cut samples were manually realigned, and nominal pressure was manually applied at the interface to ensure good contact between the pair of fractured surfaces. All

https://doi.org/10.1021/acsmaterialslett.4c01358
ACS Materials Lett. 2025, 7, 123−132

samples were allowed to rest for 5 min prior to mechanical testing to allow for viscoelastic relaxation.

Stress−strain curves from uniaxial tension testing of the pristine material (Figure 2b) exhibited typical nonlinear elastic (N-shaped) profiles, with a large compliant region from 25% to nearly 300% strain and well-defined strain-stiffening behavior at higher elongations. The material's large compliant region could be advantageous for large-deformation actuation applications, where large strains could be achieved with modest actuation forces. The high degree of strain stiffening following the compliant region is potentially useful for mitigating unintended material failure. The dehydrated material has a higher Young's modulus than the ambiently stored material due to water reducing the polymer fraction and likely interfering with interchain hydrogen bond formation. The pristine cast material exhibits robust mechanical properties, with ultimate tensile stresses (UTSs) exceeding 1.12 ± 0.56 MPa and 2.96 ± 0.14 MPa for ambient and dehydrated samples, respectively. Compared to other intrinsically self-healing photocurable elastomers, including those synthesized using custom precursors, the pristine UTS values are among the highest reported in the field (Figure S9 in the Supporting Information). Although elongation at fracture for the pristine cast material is modest (423% ± 29% for ambient and 458% ± 8% for dehydrated), compared to some of its counterparts, it is expected to provide sufficiently large elastic deformations for the vast majority of potential applications.[38]

While the mechanical properties of hydrogels with varied water content have been previously examined,[39,40] the interplay between adhesion, modulus, and water content in determining self-healing capacity has received little attention. As discussed above, increasing humidity lowered the Young's modulus of these elastomers by interfering with interchain hydrogen bonding, and this is known to increase self-healing via interdiffusion of the polymer chains.[41] However, water-based softening can have tradeoffs with hydrophilic adhesive polymer interfaces. As more water is incorporated, productive polymer−polymer hydrogen bonding is replaced with inactive polymer−solvent hydrogen bonding. To explore these relations, we compared self-healing performance in dry (that is, no water directly added) hydrogel networks exposed to different degrees of humidity (Figure 2b).

Although the self-healing efficiencies (the ratio of the healed to pristine properties) of these materials are notably less than 100%, the performance of the self-healed material is still formidable due to excellent pristine properties (Figure 2b). Ambiently stored cast samples exhibited larger strains, but lower stresses, than their dehydrated counterparts upon healing (fracture at 344 ± 18% engineering strain and 0.34 ± 0.05 MPa UTS compared to 238 ± 17% engineering strain and 0.74 ± 0.11 MPa UTS). Given the rapidity of this purely adhesive self-healing, the mechanical properties of the healed specimens are quite substantial. This material exhibits impressive strength for its rate of healing when compared to other intrinsically self-healing photocurable elastomers (Figure 2c).[23−25,29,31,41−52] This performance is especially notable when looking at the subset of reported materials that do not rely on custom synthesis to produce their resins. As a result of such rapid healing, the material reported herein is an excellent candidate for ensuring continuous functionality of printed soft devices in the event of minor damage.

DLP 3D-printed specimens exhibited different mechanical properties from their cast counterparts across all sample configurations (Figure 2b). This is likely due to pixilation defects from DLP printing, different flux and wavelength of the UV light used for curing, and shorter chain growth due to lower temperatures in the vat, compared to casting, where the bulk thermal momentum of the resin can drive rapid autopolymerization.[53] However, DLP specimens were also prepared with food dye carried by non-negligible amounts of water, which may affect polymerization. Control studies were conducted using cast samples with added water to approximate the water content in DLP resins. These samples showed a small reduction in Young's modulus and delayed onset of strain stiffening, resulting in similar failure stresses at higher strains (Figure S10 in the Supporting Information). While notable, these changes do not fully explain the differences in mechanical properties between cast and DLP samples, suggesting that pixilation and differences in polymerization conditions drive the earlier failure of DLP samples. Despite the decreases in pristine sample performance, healed DLP specimens still exhibited failure strains of 166% ± 33% for dehydrated samples and 268% ± 10% for ambiently stored samples.

Quantifying the degree of viscoelasticity exhibited by a self-healing material is critical to determining its performance in realistic applications, especially those requiring rapid responses. For the material reported herein, the degree of viscoelasticity depends significantly on water content due to the hydrogen bonding. Cyclic tension tests conducted on dehydrated cast samples revealed notable hysteresis and cycle-to-cycle softening (Figure 2d). However, tests conducted on ambiently stored samples displayed less hysteresis and weaker cycle-to-cycle softening (see Figure 2d, as well as Figure S11 in the Supporting Information). This suggests that, while the plasticizing nature of water sacrifices some strength and modulus, it helps to minimize time dependence in the material's response, likely by weakening the contribution of temporary bonds.[54] Ultimately, this more perfectly elastic (less lossy) behavior can yield devices that are more responsive to external actuation.

Long-duration humidity-controlled rheological analyses were conducted to quantify the extent that mechanical properties can be tuned with atmospheric water content (Figure 2e). Varying the humidity from 10% to 90% RH revealed an ∼60%−75% decrease in the complex shear modulus of the material (Figure S12 in the Supporting Information). The fact that the equilibration time of this material to ambient humidity is long (tens of hours) suggests that reasonable operation windows can be maintained and that mechanical properties can be significantly tuned by a given storage condition. Further temperature-controlled rheological differential scanning calorimetry testing showed that the material has a glass-transition temperature near 10 °C (see Figures S13 and S14 in the Supporting Information), with steep property modulation around room temperature. Collectively, these rheological behaviors hold capacity for on-demand property modulation using temperature and humidity control.

To evaluate the capacity for multiple healing cycles, the degradation of adhesive properties at a repeatedly grafted interface was studied (Figure 2f). Because manual realignment of samples hinders repeatability, a modified version of a probe tack test was conducted, wherein 2.1 N of compressive force was used to bring two cast samples into contact, after which they were rapidly separated. This testing revealed that even during rapid self-healing events, the ambiently stored material only lost ∼14% of the initial adhesive force it had on the first separation by the fifth healing. This minor loss of adhesive capacity is expected

https://doi.org/10.1021/acsmaterialslett.4c01358
ACS Materials Lett. 2025, 7, 123−132

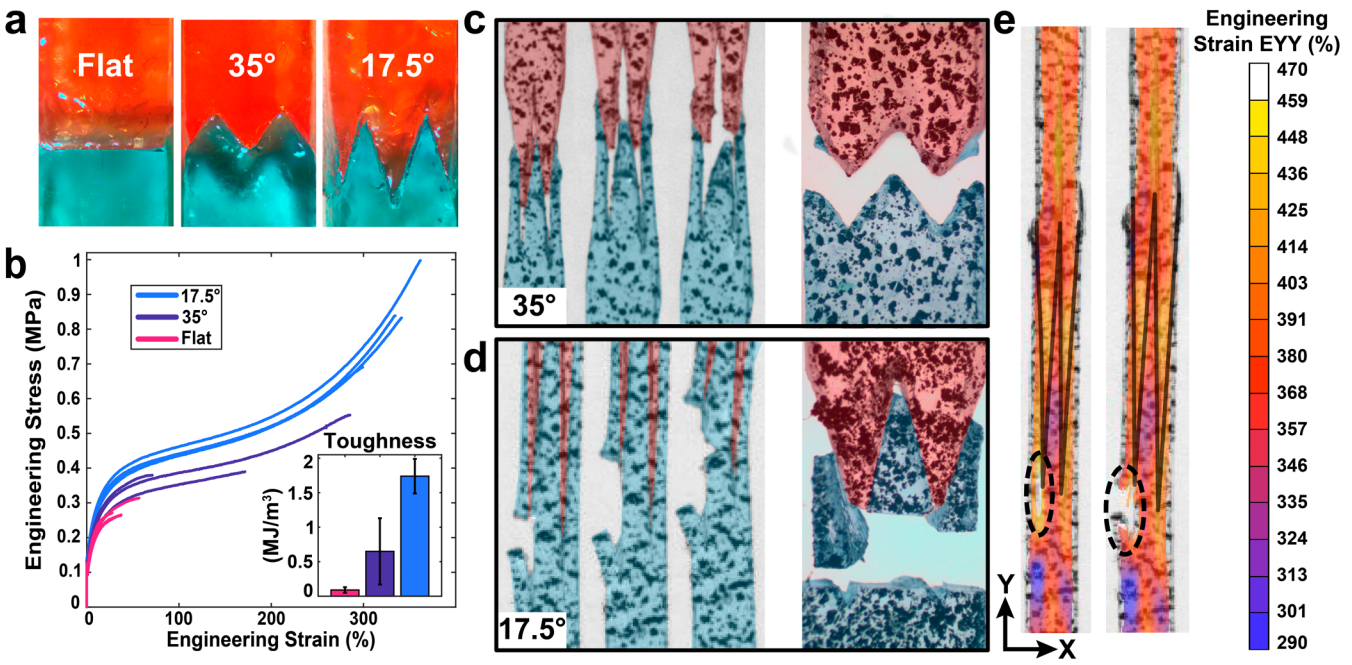

Figure 3. Effect of herringbone grafted interfaces on fracture mechanics. (a) Self-healed samples with flat and herringbone (17.5° and 35°) interfaces grafted using separately cast halves. (b) Uniaxial tension (500 mm/min ≈ 0.1/s) stress−strain curves and toughness data comparing flat and herringbone grafted interface performance on cast samples with imperfect self-healing conditions. The 17.5° interfaces increased toughness by a factor of 18, compared to flat interfaces. (c) 35° grafted tensile specimen fracture primarily due to adhesive failure. (d) 17.5° grafted tensile specimens failed cohesively straight across the healed interface. (e) DIC engineering strain measurements of a 17.5° sample revealing strain localization near the healed interface. In this sample, the strain localization at the tip of the left tooth is consistent with cohesive fracture in the material away from the healed interface.

to arise from a slight reorganization of low-molecular-weight components at the interface upon repeated compressions and separations. This retention of adhesive capacity lends the material toward use in reconfigurable devices, where multiple rapid healings can help facilitate iterative reconstruction.

STRUCTURE-ENHANCED FUNCTIONALITY

The 3D printability of the material reported herein provides an opportunity to design the mechanical interface between healable components. Unlike damage repair, material grafting can leverage fracture mechanics principles to enhance (or degrade) self-healing performance, and potentially control fracture location and morphology.[55] To evaluate this strategy, modular self-healing samples cast with different interfacial geometries were evaluated for their interfacial strength between grafted surfaces. Increasing interfacial area, and hence grafting strength, was explored with herringbone interfaces at differing acuteness measuring from 35° to 17.5° (Figure 3a). It is notable that grafted samples cast in separate halves with a flat interface experienced significantly lower self-healing (~98% reduction in toughness) than samples that were cut in half and aligned immediately afterward. We attribute this result to several possible complicating factors present during grafting. First, samples cast in separate pieces and grafted together do not experience the bond disruption that occurs during sample cutting. The persistence of stronger hydrogen-bonding complexes formed during the high temperatures of polymerization can limit cross-interface hydrogen-bond formation and polymer diffusion. Other contributing factors could include slight geometric differences between the two pieces from imperfect molding geometries and exposure to airborne particles over the week-long storage prior to testing. While all these effects can likely be mitigated,[56] we believe they are practically relevant and would likely be encountered during modular device assembly in typical uncontrolled environments.

Grafts with 35° interfaces (a moderate degree of acuteness) yielded a toughness of 0.65 ± 0.48 MJ/m^3 with strains of 176% ± 107% (Figure 3b), showing a factor of 6 increase in toughness over flat interfaces. However, as shown in Figure 3c, these samples mostly fractured adhesively along the grafted interface (although some small pieces were observed on the outer edge of their opposing graft). Increasing the acuteness of the herringbone pattern to 17.5° produced interfaces with ~3.3 times the cross-sectional area of the flat specimens (Figure S15 in the Supporting Information). In these specimens, fracture consistently occurred away from the grafted interface (Figure 3d), indicating that the engineered graft effectively changes the path of lowest fracture energy to be horizontally across the sample and not at the self-healed interface. Despite meaningfully enhancing the healed material performance, strain localization at the herringbone teeth leads to fracture initiation before the pristine material properties are reached by the bulk sample (Figure 3e). The strain localization appeared early in the testing at the interface between the teeth, likely due to imperfections in the alignment and geometry between the two faces (Figure S16 in the Supporting Information). The fracture events in the 17.5° sample originated at a strain localization with peaks of approximately 460%, a failure strain that aligns well with pristine uniaxial tension failures in cast dehydrated samples (see Video S2 in the Supporting Information).

The strong performance enhancement and repeatability of the grafts over many samples demonstrates that engineered interfaces can be used to boost a material's "effective" self-healing efficiency (Figure S17 in the Supporting Information).

https://doi.org/10.1021/acsmaterialslett.4c01358
ACS Materials Lett. 2025, 7, 123−132

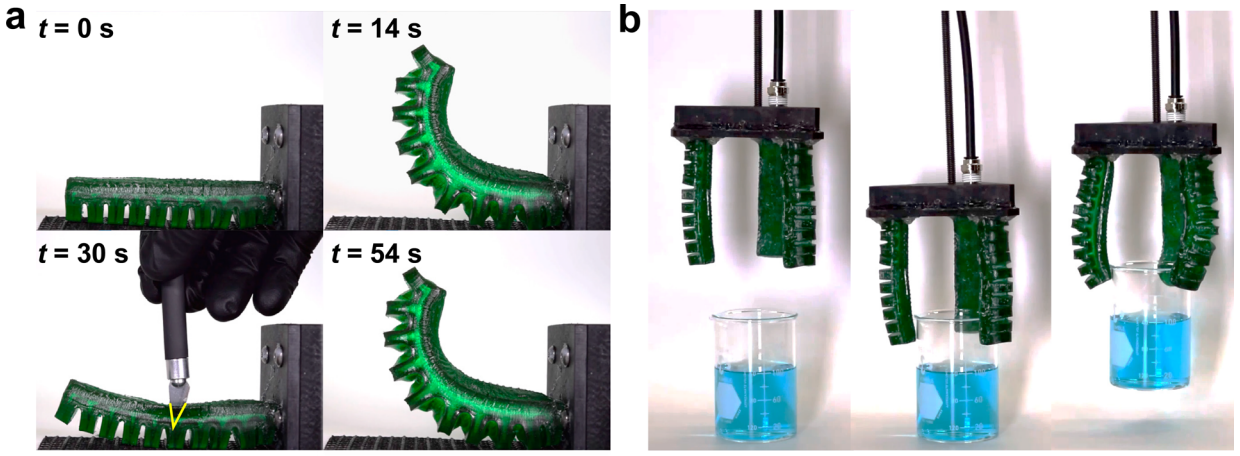

Figure 4. Pneumatic actuation and rapid, autonomous self-healing. (a) Dehydrated 3D-printed actuator is actuated to ∼1.5 psi, punctured with a blade, and reactuated immediately following the removal of the knife. No manual realignment or external stimulus is needed to facilitate the healing reaction. (b) Three-fingered, 3D-printed gripper is actuated to successfully lift a 165-g glass beaker of water (dyed blue). Polytetrafluoroethylene (PTFE) spray was applied to the fingers prior to testing to minimize the contribution of surface adhesion to lifting capacity.

In fact, the 17.5° samples reported the best self-healing performance in this work, with an impressive toughness of 1.74 ± 0.25 MJ/m^3, ∼18 times greater than that of flat interfaces. The increased shear resistance along the teeth due to transverse compressive deformations (arising from the Poisson effect) and the larger contact area (which increases with strain productively due to rapid self-healing) are believed to be the primary drivers of the enhanced self-healing. The extent that these mechanisms can boost self-healing performance surpasses previous studies of similar grafting geometries reported in the literature.[57] Although the fracture modes (cohesive and adhesive) and fracture locations resemble those of suture and wood finger joints,[58−60] the effects of large-deformation kinematics and hyperelastic material behavior likely result in the material's divergence from the performance predictions of previous grafted interface models, which are restricted to small strains and linear elastic response regimes.

The large increases in toughness accessible with only modest structuring in these grafted interfaces offers a path to utilize practical materials with modest self-healing capacity that would otherwise be overlooked. Furthermore, grafted interfaces provide a route to fabricate multimaterial devices using techniques (e.g., vat photopolymerization) that would otherwise be unable to produce such structures in situ. Grafts can also serve as important tools for ensuring proper alignment of small features (e.g., air chambers) and for developing reconfigurable soft devices.[61,62] Continued research of grafted interfaces could help self-healing materials find application in real-world scenarios by compensating for external contaminants, poor self-healing capacity, misalignment, and print defects—all of which are capable of derailing even the most robust self-healing materials.

SOFT ROBOTIC DEMONSTRATORS

To demonstrate the elastomer's ability to rapidly and autonomously repair damage, a simple pneumatic actuator was designed and 3D printed (Figure S18 in the Supporting Information). The pneumatic actuator is composed of 10 bellows connected by a central air chamber spanning the length of the device. After printing, the soft device was post-cured, stored for 1 week in a nitrogen-purged desiccator, and treated with a nonstick polytetrafluoroethylene (PTFE) spray to make it easier to handle. The actuator was connected to a custom fixture using a gasket printed at the end of the robot, and then actuated with compressed air at a pressure of ∼1.5 psi. After deflation to nominally 0 psi, a ∼7-mm-long puncture was created with an X-Acto knife (Figure 4a). The actuator was then successfully reinflated under 1.5 psi of compressed air pressure to its previous deformed position (see Note S3 and Video S3 in the Supporting Information). This result demonstrates how the actuator is able to autonomously self-heal without human realignment in seconds due to rapid hydrogen bonding at the adhesion site. It is notable that the air leakage present when the knife was inserted stopped almost immediately after the blade was removed.

To demonstrate the suitability of these materials for soft robotic applications, three identical actuators were attached to a custom fixture to form a three-finger gripper (Figure 4b). The soft robotic gripper was placed around a 150 mL glass beaker filled with 100 mL of water (dyed blue) with a net weight of 165 g. Manually placing the fingers on the rim of the beaker and actuating to ∼1.5 psi was sufficient to grasp and elevate the beaker. The security of the grip was tested by moving the lifted beaker laterally for several seconds before finally releasing the beaker (Video S4 in the Supporting Information). The ease of release indicates that adhesive forces did not play a meaningful role in suspending the beaker. The successful three-finger gripper demonstrates that the material has suitable mechanical properties to serve as an effective soft robotic actuator. With improved actuator and fixture design, it is likely that the gripper's lift capacity could be increased significantly. To support this notion, we note that water-filled beakers weighing nearly 500 g were successfully lifted during our gripping experiments.

The DLP-compatible material developed in this work bridges the gap between rapidly self-healing elastomers, commercial-scale resin printing, and simple synthesis using COTS precursors. The powerful combination of these features was enabled by a novel hybrid acrylate/thiol-ene formulation with low viscosity, well suited for DLP printing. DLP print capability encourages innovative designs and wider-scale adoption of self-healing soft materials by enabling geometries with complex form factors and manufacturing scalability. With a reported pristine

https://doi.org/10.1021/acsmaterialslett.4c01358
ACS Materials Lett. 2025, 7, 123−132

toughness of 4.60 ± 0.49 MJ/m^3, the material reported herein challenges the notion that tedious and expensive synthesis is required to achieve attractive mechanical properties in printable self-healing materials.

Engineered herringbone grafts were used to drive fracture away from healed interfaces and improve self-healed toughness by a factor of 18. This indicates that interfacial design can be leveraged to overcome mechanical property limitations, suggesting that materials with only modest self-healing capacity can be facilely structured to fail away from grafted interfaces and realize order-of-magnitude increases in toughness post-healing with only modest increases in interfacial surface area. Furthermore, our material's 3D printability affords compelling flexibility for exploring more intricate grafted interface designs.

A pneumatic three-finger gripper was 3D printed and shown to successfully lift a 165-g water-filled beaker. Furthermore, a 3D-printed single-finger gripper rapidly and autonomously self-healed a 7-mm-long puncture inflicted during operation. This demonstration of continuous functionality and lack of intervention during damage repair represents a meaningful step toward soft devices capable of thriving in remote natural environments, industrial agricultural settings, and extraterrestrial conditions.

EXPERIMENTAL METHODS

Casting. Cast samples were cured with an LED power supply (CF2000, Clearstone) equipped with a 365 nm bulb (JL1 Series 365E-48). The power supply's UV unit was positioned 25 cm above the top of the mold and set to 25% power. A power meter (UP19K-15S−H5-DO, Gentec-EO) measured a peak flux of 2.9 mW/cm^2 at a wavelength of 365 nm directly under the UV source. Further experimental details are provided in the Supporting Information.

3D Printing. A stock 3D Systems Figure 4 Modular DLP printer with no physical alterations was used for 3D printing (see Note S6 in the Supporting Information). A 50-μm layer thickness was used in the prints with an 11.27 s cure time for each layer. The UV sources provided a UV flux of 19.07 mW/m^2 at a peak wavelength of 408 nm, as measured using a digital spectrometer (BLACK-Comet, StellarNet, Inc.). All printed parts were cleaned using 99% IPA. A 5 min post-cure (300−550 nm) in a UV print box (LC-3DPrint Box, NextDent) was applied to all DLP-printed parts (see Note S7 in the Supporting Information). Further experimental details are provided in the Supporting Information.

Mechanical Characterization. Quasi-static uniaxial tension testing was conducted on an Instron 3365 extended-height load frame with a 2-kN Instron load cell for force measurement. Strain measurements were provided by an Instron long-travel clip-on extensometer. All tensile specimens adhered to ASTM D412 type C specimen dimensions. Unless otherwise stated, all uniaxial tensile tests were conducted at 500 mm/min, following the ASTM D412 test standard. Cyclic tension tests were conducted over the course of five displacement-controlled cycles between crosshead displacements of 0 and 190 mm.

To conduct self-healing tests, tension specimens were cut using a clean razor blade. Samples were allowed to rest for 5 min prior to realignment by hand. All DIC images were taken using a machine vision camera (Model BFS-U3-88S6M-C, FLIR) with a 35 mm focal length lens (HP series, Edmund Optics). Further experimental details are provided in the Supporting Information.

Elastomer Rheology and Modified Probe Tack Test. All rheological testing was conducted on 2-mm-thick/25-mm-diameter cast disks of dehydrated material. Humidity and temperature sweeps were performed using an Anton Paar MCR 702 MultiDrive with 25 mm parallel plates (L-PP25/TD/TS) with a CTD180 HR convection oven and an MHG 100 humidity generator. For repeated self-healing tests (using a modified probe tack test), a TA Instruments RSA-G2 solids analyzer with 25 mm steel parallel plates was used. For each cycle, the samples were compressed to 2.1 N, allowed to rest for 1 s, and rapidly separated at a rate of 10 mm/min. Each sample underwent five compressive cycles. Further experimental details are provided in the Supporting Information.

ASSOCIATED CONTENT

Data Availability Statement

The data that support the findings of this study are openly available in the University of Dayton eCommons institutional repository at https://ecommons.udayton.edu/selfhealing_elastomer.

Supporting Information

The Supporting Information is available free of charge at https://pubs.acs.org/doi/10.1021/acsmaterialslett.4c01358.

Additional experimental details, methods, and results, including cast and 3D-printed resin composition; resin storage; print resolution studies; variation of mechanical response with water content; rheological analyses of cured resin; and DSC, FTIR, TGA, and rheological analysis of uncured resin (PDF)

Time-lapse recording of a large gyroid lattice DLP print (Video S1) (MP4)

Strain localization in a 35° grafted specimen leading to cohesive fracture (Video S2) (AVI)

Real-time autonomous self-healing of a soft robotic actuator (Video S3) (MP4)

Soft robotic gripper lifts and releases beaker (Video S4) (MP4)

AUTHOR INFORMATION

Corresponding Authors

Carl J. Thrasher − *Department of Materials Science and Engineering, Massachusetts Institute of Technology, Cambridge, Massachusetts 02142, United States*; Email: cthrash@mit.edu

Robert L. Lowe − *Department of Mechanical and Aerospace Engineering, University of Dayton, Dayton, Ohio 45469, United States*; orcid.org/0000-0002-4997-5584; Email: robert.lowe@udayton.edu

Christopher A. Crouse − *Air Force Research Laboratory, Materials and Manufacturing Directorate, Wright-Patterson AFB, Ohio 45433, United States*; orcid.org/0009-0001-6567-3957; Email: christopher.crouse.1@us.af.mil

Authors

Joseph G. Beckett − *Department of Mechanical and Aerospace Engineering, University of Dayton, Dayton, Ohio 45469, United States; UES, Inc., Dayton, Ohio 45432, United States*; Present Address: Department of Mechanical Engineering, University of Michigan, Ann Arbor, MI 48109, USA

Joshua Michonski − *Department of Mechanical and Aerospace Engineering, University of Dayton, Dayton, Ohio 45469, United States; UES, Inc., Dayton, Ohio 45432, United States*

https://doi.org/10.1021/acsmaterialslett.4c01358
ACS Materials Lett. 2025, 7, 123−132

Robert M. Drexler − *Department of Mechanical and Aerospace Engineering, University of Dayton, Dayton, Ohio 45469, United States; UES, Inc., Dayton, Ohio 45432, United States*
Sachin Babu − *UES, Inc., Dayton, Ohio 45432, United States; Air Force Research Laboratory, Materials and Manufacturing Directorate, Wright-Patterson AFB, Ohio 45433, United States*
Allyson M. Cox − *Additive Manufacturing Technology Development, University of Dayton Research Institute, Dayton, Ohio 45469, United States*
Braeden J. Windham − *Additive Manufacturing Technology Development, University of Dayton Research Institute, Dayton, Ohio 45469, United States*
Zhenning Yu − *UES, Inc., Dayton, Ohio 45432, United States; Air Force Research Laboratory, Materials and Manufacturing Directorate, Wright-Patterson AFB, Ohio 45433, United States*
Anesia D. Auguste − *Air Force Research Laboratory, Materials and Manufacturing Directorate, Wright-Patterson AFB, Ohio 45433, United States*
Abhishek Shetty − *Anton Paar USA, Inc., Ashland, Virginia 23005, United States*
Timothy H. Osborn − *Additive Manufacturing Technology Development, University of Dayton Research Institute, Dayton, Ohio 45469, United States*
Laura A. Sowards − *Air Force Research Laboratory, Materials and Manufacturing Directorate, Wright-Patterson AFB, Ohio 45433, United States*

Complete contact information is available at:
https://pubs.acs.org/10.1021/acsmaterialslett.4c01358

Author Contributions

CRediT: **Joseph G. Beckett** conceptualization, data curation, formal analysis, investigation, methodology, validation, visualization, writing - original draft, writing - review & editing; **Carl J. Thrasher** conceptualization, formal analysis, investigation, methodology, visualization, writing - original draft, writing - review & editing; **Joshua Michonski** data curation, formal analysis, investigation, methodology, validation; **Robert M. Drexler** investigation, validation; **Sachin Babu** investigation; **Allyson M. Cox** investigation, methodology, supervision; **Braeden J. Windham** investigation, methodology; **Zhenning Yu** investigation; **Anesia D. Auguste** formal analysis, investigation, methodology, writing - review & editing, supervision; **Abhishek Shetty** investigation; **Timothy H. Osborn** project administration, resources, funding acquisition; **Robert L. Lowe** conceptualization, funding acquisition, project administration, resources, supervision, writing - review & editing; **Laura A. Sowards** funding acquisition, project administration, resources, supervision; **Christopher A. Crouse** conceptualization, funding acquisition, project administration, resources, supervision, writing - review & editing.

Notes

The authors declare no competing financial interest.

■ ACKNOWLEDGMENTS

R.L. would like to acknowledge support from the AFRL Materials and Manufacturing Directorate through the AFOSR Summer Faculty Fellowship Program (Contract Nos. FA8750-15-3-6003, FA9550-15-0001, and FA9550-20-F-0005). R.L. also acknowledges support from the NSF Major Research Instrumentation Program (Grant No. MRI-2216191). J.B. and J.M. are grateful for support from a NASA/Ohio Space Grant Consortium Undergraduate STEM Scholarship. J.B. acknowledges support from the National Defense Science and Engineering Graduate Fellowship Program as well as the Barry Goldwater Scholarship & Excellence in Education Foundation. J.B. and R.D. thank the University of Dayton Berry Summer Thesis Institute for summer research support. B.W. thanks the University of Dayton SURE Program for financial support. The authors would like to thank Dr. Vincent Chen, Dr. Bingqian Zheng, James Denault, and Grant Eifert for their technical contributions and support. Distribution A: Approved for public release; distribution is unlimited (PA No. AFRL-2023-3243).

■ REFERENCES

(1) Patterson, Z.; Patel, D.; Bergbreiter, S.; Yao, L.; Majidi, C. A method for 3D printing and rapid prototyping of fieldable untethered soft robots. *Soft Robot.* **2023**, *10*, 292−300.
(2) Cvetkovic, C.; Raman, R.; Chan, V.; Williams, B.; Tolish, M.; Bajaj, P.; Sakar, M.; Asada, H.; Saif, M.; Bashir, R. Three-dimensionally printed biological machines powered by skeletal muscle. *Proc. Natl. Acad. Sci. U. S. A.* **2014**, *111*, 10125−10130.
(3) Keplinger, C.; Sun, J.-Y.; Foo, C.; Rothemund, P.; Whitesides, G.; Suo, Z. Stretchable, transparent, ionic conductors. *Science* **2013**, *341*, 984−987.
(4) Guo, S.-Z.; Qiu, K.; Meng, F.; Park, S.; McAlpine, M. 3D printed stretchable tactile sensors. *Adv. Mater.* **2017**, *29*, 1701218.
(5) Lee, K.; Mooney, D. Hydrogels for tissue engineering. *Chem. Rev.* **2001**, *101*, 1869−1880.
(6) Anderson, I.; Gisby, T.; McKay, T.; O'Brien, B.; Calius, E. Multi-functional dielectric elastomer artificial muscles for soft and smart machines. *J. Appl. Phys.* **2012**, *112*, 041101.
(7) Lee, Y.; Cha, S.; Kim, Y.-W.; Choi, D.; Sun, J.-Y. Transparent and attachable ionic communicators based on self-cleanable triboelectric nanogenerators. *Nat. Commun.* **2018**, *9*, 1804.
(8) Blaiszik, B.; Kramer, S.; Olugebefola, S.; Moore, J.; Sottos, N.; White, S. Self-healing polymers and composites. *Annu. Rev. Mater. Res.* **2010**, *40*, 179−211.
(9) Kang, J.; Son, D.; Vardoulis, O.; Mun, J.; Matsuhisa, N.; Kim, Y.; Kim, J.; Tok, J. B.-H.; Bao, Z. Modular and reconfigurable stretchable electronic systems. *Adv. Mater. Technol.* **2019**, *4*, 1800417.
(10) Xu, R.; Cañón Bermúdez, G.; Pylypovskyi, O.; Volkov, O.; Oliveros Mata, E.; Zabila, Y.; Illing, R.; Makushko, P.; Milkin, P.; Ionov, L.; Fassbender, J.; Makarov, D. Self-healable printed magnetic field sensors using alternating magnetic fields. *Nat. Commun.* **2022**, *13*, 6587.
(11) Zhang, L.; Liu, Z.; Wu, X.; Guan, Q.; Chen, S.; Sun, L.; Guo, Y.; Wang, S.; Song, J.; Jeffries, E.; et al. A highly efficient self-healing elastomer with unprecedented mechanical properties. *Adv. Mater.* **2019**, *31*, 1901402.
(12) Terryn, S.; Brancart, J.; Lefeber, D.; Van Assche, G.; Vanderborght, B. Self-healing soft pneumatic robots. *Sci. Robot.* **2017**, *2*, eaan4268.
(13) Wang, H.; Terryn, S.; Wang, Z.; Van Assche, G.; Iida, F.; Vanderborght, B. Self-Regulated self-healing robotic gripper for resilient and adaptive grasping. *Adv. Intell. Syst.* **2023**, *5*, 2300223.
(14) Yao, W.; Tian, Q.; Shi, J.; Luo, C.; Wu, W. Printable, down/up-conversion triple-mode fluorescence responsive and colorless self-healing elastomers with superior toughness. *Adv. Funct. Mater.* **2021**, *31*, 2100211.
(15) Roppolo, I.; Caprioli, M.; Pirri, C.; Magdassi, S. 3D printing of self-healing materials. *Adv. Mater.* **2024**, *36*, 2305537.
(16) Kuang, X.; Chen, K.; Dunn, C. K.; Wu, J.; Li, V. C. F.; Qi, H. J. 3D printing of highly stretchable, shape-memory, and self-healing elastomer toward novel 4D printing. *ACS Appl. Mater. Interfaces* **2018**, *10*, 7381−7388.
(17) Lai, J.; Wang, X.; Zhao, Q.; Zhang, C.; Gong, T.; He, L.; Wang, Z.; Xia, H. 3D printing self-healing and self-adhesive elastomers for wearable electronics in amphibious environments. *ACS Appl. Mater. Interfaces* **2024**, *16*, 16880−16892.

(18) Kim, M.; Nian, S.; Rau, D. A.; Huang, B.; Zhu, J.; Freychet, G.; Zhernenkov, M.; Cai, L.-H. 3D printable modular soft elastomers from physically cross-linked homogeneous associative polymers. *ACS Polym. Au* **2024**, *4*, 98.
(19) Roels, E.; Terryn, S.; Iida, F.; Bosman, A.; Norvez, S.; Clemens, F.; Van Assche, G.; Vanderborght, B.; Brancart, J. Processing of self-healing polymers for soft robotics. *Adv. Mater.* **2022**, *34*, 2104798.
(20) Thrasher, C.; Schwartz, J.; Boydston, A. Modular elastomer photoresins for digital light processing additive manufacturing. *ACS Appl. Mater. Interfaces* **2017**, *9*, 39708−39716.
(21) Fang, Z.; Mu, H.; Sun, Z.; Zhang, K.; Zhang, A.; Chen, J.; Zheng, N.; Zhao, Q.; Yang, X.; Liu, F.; Wu, J.; Xie, T. 3D printable elastomers with exceptional strength and toughness. *Nature* **2024**, *631*, 783−788.
(22) Taylor, D.; in het Panhuis, M. Self-healing hydrogels. *Adv. Mater.* **2016**, *28*, 9060−9093.
(23) Li, X.; Yu, R.; He, Y.; Zhang, Y.; Yang, X.; Zhao, X.; Huang, W. Self-healing polyurethane elastomers based on a disulfide bond by digital light processing 3D printing. *ACS Macro Lett.* **2019**, *8*, 1511−1516.
(24) Gong, H.; Gao, Y.; Jiang, S.; Sun, F. Photocured materials with self-healing function through ionic interactions for flexible electronics. *ACS Appl. Mater. Interfaces* **2018**, *10*, 26694−26704.
(25) Durand-Silva, A.; Cortés-Guzmán, K.; Johnson, R.; Perera, S.; Diwakara, S.; Smaldone, R. Balancing self-healing and shape stability in dynamic covalent photoresins for stereolithography 3D printing. *ACS Macro Lett.* **2021**, *10*, 486−491.
(26) Xu, J.; Zhu, L.; Nie, Y.; Li, Y.; Wei, S.; Chen, X.; Zhao, W.; Yan, S. Advances and challenges of self-healing elastomers: a mini review. *Materials* **2022**, *15*, 5993.
(27) Zhang, Z.; Ghezawi, N.; Li, B.; Ge, S.; Zhao, S.; Saito, T.; Hun, D.; Cao, P.-F. Autonomous self-healing elastomers with unprecedented adhesion force. *Adv. Funct. Mater.* **2021**, *31*, 2006298.
(28) Wallin, T.; Pikul, J.; Bodkhe, S.; Peele, B.; Mac Murray, B.; Therriault, D.; McEnerney, B.; Dillon, R.; Giannelis, E.; Shepherd, R. Click chemistry stereolithography for soft robots that self-heal. *J. Mater. Chem. B* **2017**, *5*, 6249−6255.
(29) Gomez, E.; Wanasinghe, S.; Flynn, A.; Dodo, O.; Sparks, J.; Baldwin, L.; Tabor, C.; Durstock, M.; Konkolewicz, D.; Thrasher, C. 3D-printed self-healing elastomers for modular soft robotics. *ACS Appl. Mater. Interfaces* **2021**, *13*, 28870−28877.
(30) Desroches, G.; Thrasher, C.; Diaco, N.; Raji, I.; Konkolewicz, D.; Hart, A.; Macfarlane, R. Multivalent polymer-grafted nanoparticles as reinforcing fillers for 3D printable self-healing elastomers. *ACS Mater. Lett.* **2024**, *6*, 4175−4182.
(31) Wanasinghe, S.; Johnson, B.; Revadelo, R.; Eifert, G.; Cox, A.; Beckett, J.; Osborn, T.; Thrasher, C.; Lowe, R.; Konkolewicz, D. 3D printable adhesive elastomers with dynamic covalent bond rearrangement. *Soft Matter* **2023**, *19*, 4964−4971.
(32) Cui, J.; del Campo, A. Multivalent H-bonds for self-healing hydrogels. *Chem. Commun.* **2012**, *48*, 9302−9304.
(33) Xie, Z.; Hu, B.-L.; Li, R.-W.; Zhang, Q. Hydrogen bonding in self-healing elastomers. *ACS Omega* **2021**, *6*, 9319−9333.
(34) Faghihnejad, A.; Feldman, K.; Yu, J.; Tirrell, M.; Israelachvili, J.; Hawker, C.; Kramer, E.; Zeng, H. Adhesion and surface interactions of a self-healing polymer with multiple hydrogen-bonding groups. *Adv. Funct. Mater.* **2014**, *24*, 2322−2333.
(35) Zhang, B.; Digby, Z.; Flum, J.; Chakma, P.; Saul, J.; Sparks, J.; Konkolewicz, D. Dynamic thiol−Michael chemistry for thermoresponsive rehealable and malleable networks. *Macromolecules* **2016**, *49*, 6871−6878.
(36) Chen, L.; Wu, Q.; Wei, G.; Liu, R.; Li, Z. Highly stable thiol−ene systems: from their structure−property relationship to DLP 3D printing. *J. Mater. Chem. C* **2018**, *6*, 11561−11568.
(37) Al-Ketan, O.; Abu Al-Rub, R. MSLattice: A free software for generating uniform and graded lattices based on triply periodic minimal surfaces. *Mater. Des. Process. Commun.* **2021**, *3*, e205.
(38) Wallin, T.; Pikul, J.; Shepherd, R. 3D printing of soft robotic systems. *Nat. Rev. Mater.* **2018**, *3*, 84−100.
(39) Oyen, M. Mechanical characterisation of hydrogel materials. *Int. Mater. Rev.* **2014**, *59*, 44−59.
(40) Anseth, K.; Bowman, C.; Brannon-Peppas, L. Mechanical properties of hydrogels and their experimental determination. *Biomaterials* **1996**, *17*, 1647−1657.
(41) Caprioli, M.; Roppolo, I.; Chiappone, A.; Larush, L.; Pirri, C.; Magdassi, S. 3D-printed self-healing hydrogels via digital light processing. *Nat. Commun.* **2021**, *12*, 2462.
(42) Liu, Z.; Hong, P.; Huang, Z.; Zhang, T.; Xu, R.; Chen, L.; Xiang, H.; Liu, X. Self-healing, reprocessing and 3D printing of transparent and hydrolysis-resistant silicone elastomers. *Chem. Eng. J.* **2020**, *387*, 124142.
(43) Yu, K.; Xin, A.; Du, H.; Li, Y.; Wang, Q. Additive manufacturing of self-healing elastomers. *NPG Asia Mater.* **2019**, *11*, 7.
(44) Guo, B.; Ji, X.; Chen, X.; Li, G.; Lu, Y.; Bai, J. A highly stretchable and intrinsically self-healing strain sensor produced by 3D printing. *Virtual Phys. Prototyping* **2020**, *15*, 520−531.
(45) Wu, Y.; Zeng, Y.; Chen, Y.; Li, C.; Qiu, R.; Liu, W. Photocurable 3D printing of high toughness and self-healing hydrogels for customized wearable flexible sensors. *Adv. Funct. Mater.* **2021**, *31*, 2107202.
(46) Cheng, K.; Chortos, A.; Lewis, J.; Clarke, D. Photoswitchable covalent adaptive networks based on thiol−ene elastomers. *ACS Appl. Mater. Interfaces* **2022**, *14*, 4552−4561.
(47) Wei, Y.; Xiang, L.; Ou, H.; Li, F.; Zhang, Y.; Qian, Y.; Hao, L.; Diao, J.; Zhang, M.; Zhu, P.; et al. MXene-based conductive organohydrogels with long-term environmental stability and multifunctionality. *Adv. Funct. Mater.* **2020**, *30*, 2005135.
(48) Wang, W.; Liu, S.; Liu, L.; Alfarhan, S.; Jin, K.; Chen, X. High-speed and high-resolution 3D printing of self-healing and ion-conductive hydrogels via μCLIP. *ACS Mater. Lett.* **2023**, *5*, 1727−1737.
(49) Wu, Y.; Fei, M.; Chen, T.; Li, C.; Wu, S.; Qiu, R.; Liu, W. Photocuring three-dimensional printing of thermoplastic polymers enabled by hydrogen bonds. *ACS Appl. Mater. Interfaces* **2021**, *13*, 22946−22954.
(50) Wu, Q.; Han, S.; Zhu, J.; Chen, A.; Zhang, J.; Yan, Z.; Liu, J.; Huang, J.; Yang, X.; Guan, L. Stretchable and self-healing ionic conductive elastomer for multifunctional 3D printable sensor. *Chem. Eng. J.* **2023**, *454*, 140328.
(51) Wang, Z.; Cui, H.; Liu, M.; Grage, S.; Hoffmann, M.; Sedghamiz, E.; Wenzel, W.; Levkin, P. Tough, transparent, 3D-printable, and self-healing poly(ethylene glycol)-gel (PEGgel). *Adv. Mater.* **2022**, *34*, 2107791.
(52) Mogli, G.; Reina, M.; Chiappone, A.; Lamberti, A.; Pirri, C.; Roppolo, I.; Stassi, S. Self-powered integrated tactile sensing system based on ultrastretchable, self-healing and 3D printable ionic conductive hydrogel. *Adv. Funct. Mater.* **2024**, *34*, 2307133.
(53) Rehbein, T.; Johlitz, M.; Lion, A.; Sekmen, K.; Constantinescu, A. Temperature- and degree of cure-dependent viscoelastic properties of photopolymer resins used in digital light processing. *Progress Additive Manuf.* **2021**, *6*, 743−756.
(54) Bennett, C.; Hayes, P. J.; Thrasher, C. J.; Chakma, P.; Wanasinghe, S. V.; Zhang, B.; Petit, L. M.; Varshney, V.; Nepal, D.; Sarvestani, A.; Picu, C. R.; Sparks, J. L.; Zanjani, M. B.; Konkolewicz, D. Modeling approach to capture hyperelasticity and temporary bonds in soft polymer networks. *Macromolecules* **2022**, *55*, 3573−3587.
(55) Hwang, D.; Lee, C.; Yang, X.; Pérez-González, J.; Finnegan, J.; Lee, B.; Markvicka, E.; Long, R.; Bartlett, M. Metamaterial adhesives for programmable adhesion through reverse crack propagation. *Nat. Mater.* **2023**, *22*, 1030−1038.
(56) Wilkes, G.; Wildnauer, R. Kinetic behavior of the thermal and mechanical properties of segmented urethanes. *J. Appl. Phys.* **1975**, *46*, 4148−4152.
(57) Li, Y.; Ortiz, C.; Boyce, M. A generalized mechanical model for suture interfaces of arbitrary geometry. *J. Mech. Phys. Solids* **2013**, *61*, 1144−1167.
(58) Smardzewski, J. Distribution of stresses in finger joints. *Wood Sci. Technol.* **1996**, *30*, 477−489.

https://doi.org/10.1021/acsmaterialslett.4c01358
ACS Materials Lett. 2025, 7, 123−132

(59) Özçifçi, A.; Yapící, F. Structural performance of the finger-jointed strength of some wood species with different joint configurations. *Construct. Build. Mater.* **2008**, *22*, 1543−1550.
(60) Habipi, B.; Ajdinaj, D. Wood finger-joint strength as function of finger length and slope positioning of tips. *Int. J. Eng. Appl. Sci.* **2015**, *2*, 128−132.
(61) Zhang, C.; Zhu, P.; Lin, Y.; Jiao, Z.; Zou, J. Modular soft robotics: Modular units, connection mechanisms, and applications. *Adv. Intell. Syst.* **2020**, *2*, 1900166.
(62) Lee, J.-Y.; Kim, W.-B.; Choi, W.-Y.; Cho, K.-J. Soft robotic blocks: Introducing SoBL, a fast-build modularized design block. *IEEE Robot. Automat. Mag.* **2016**, *23*, 30−41.

https://doi.org/10.1021/acsmaterialslett.4c01358
ACS Materials Lett. 2025, 7, 123−132